Alignability maps for ensuring high-precision localization

Manuel Castellano-Quero,[1] Tomasz Piotr Kucner,[2,3] and Martin Magnusson[1]

***Abstract*— Localization methods for mobile robots have been proven to work successfully in a wide variety of situations. However, there still exist certain conditions that may lead these methods to fail when deployed in real-world contexts. One of the most common issues is the scarcity of geometric features in the environment, especially for those methods relying on laser-based sensory information. In this paper, we present a map that aims to spatially capture the risk of getting localization errors. We base our proposal on a so-called alignability metric, which represents the capacity of a given range scan to be aligned with subsequent ones. In our tests, we demonstrate that the proposed alignability map serves to predict the quality of localization throughout a warehouse environment including long aisles and that the amount of visible features from a given position has a decisive impact on localization error.**

I. INTRODUCTION

Ensuring precise mobile robot localization is essential to many real-world applications, including a variety of different tasks related to industrial, domestic, medical and even search and rescue scopes. Despite the demonstrated success, even state-of-the-art localization methods may fail or work poorly in certain situations for different reasons, e.g., due to inadequate or insufficient visible landmarks [1]. Localization methods such as variants of Monte Carlo localization (MCL) rely on alignment of the current range scan to a map; but to ensure high precision, the scan data needs to be constrained enough, which essentially depends on the amount of visible geometric features. In addition, the capacity of alignment between subsequent scans is usually considered to be related to the risk of localization failure, i.e., to the risk of getting localization errors [2, 3].

Our aim in this work is to spatially represent such localization risk, particularly for laser-based localization methods that rely on existing maps. For that, we have employed a metric related to scan alignment presented by Nobili et al. [2], that can be obtained without tedious training and/or parameter tuning processes. This metric is aimed at capturing the variety of normal directions of the surfaces present in a given scan, on a zero-to-one scale. Intuitively, the greater this value is, the more constrained the alignment between different scans will be, and therefore, the lower the risk of localization failure.

In order to enable spatial prediction of localization errors in a given environment, we introduce in this paper a so-called *alignability map*, based on the alignability metric by Nobili et al. [2]. Our proposal consists in a grid map in which each cell represents the expected alignability that can be obtained from different scans at that point. Our experiments show that alignability can be employed as an indicator of the expected magnitude of localization error, and demonstrate that our approach serves to adequately anticipate such errors. A use case for the alignability maps could be, for instance, to include them as cost maps for a motion planner, which could then take localization risk into account when planning paths through feature-sparse environments.

In summary, the overall contributions of the paper are: (1) an algorithm for building alignability maps and (2), a validation of their application to the prediction of localization errors.

[1]AASS MRO lab, Örebro University, Sweden
[2]Aalto University, Finland
[3]Finnish Center for Artficial Inteligence (FCAI), Finland
Corresponding author manuel.castellano-quero@oru.se

II. RELATED WORK

Assessing the quality of localization is a topic of high relevance in robotics research, as the accuracy of state-of-the-art localization methods inevitably depends on several external factors, including the shape of the environment [4]. There exist several works in the literature that focus on defining and evaluating different indicators related to the quality of localization, which we discuss in this section.

In the scope of localization with range sensors, for instance, some works are aimed at the assessment of alignment quality between consecutive scans, which is usually addressed by developing methods for the detection of alignment errors, identified in these works as a symptom of localization failure. A typical solution consists in using the cost function of some scan registration method along with the setting of an appropriate threshold to estimate alignment quality [5, 6]. However, it is not generally possible to set a single threshold that can be applied in different environments [7]. There also exist other works that are aimed at a more elaborated fault detection of scan alignment. Bogoslavskyi and Stachniss [8], for instance, propose a quality metric based on free-space information for assessing scan matching quality, although they restrict to objects segmented in a scene. From a more generic perspective, Yin et al. [9] introduces a method based on logistic regression and metrics related to point cloud overlap and similarity for the classification of alignment errors. Almqvist et al. [7] study a number of "weak" alignment classifiers and combine them with AdaBoost. Akai et al. [10] propose a probabilistic model of scan misalignment based on Markov Random Fields (MRFs) that achieves good classification accuracy. Adolfsson et al. [11] propose to use the differential entropy in the point clouds obtained from scans for measuring alignment quality, also achieving high classification accuracy and a high degree of generalization.

The contributions mentioned so far address the alignment quality of scans "after the fact," that is, as a way to assess how well-aligned two scans actually are. In contrast, what is needed to produce a map that can predict localization error is rather a method capable of *predicting* the degree of alignability of scans instead, which is considered closely related to localization failure. Nubert et al. [12] propose a neural network-based method for detecting poor alignability of input point clouds during robot operation. Although effective, this approach requires environment-specific threshold tuning and the prediction provided is binary, meaning that different levels of localization risk would not be available, which we need in this work. An alternative solution to this approach is the one by Nobili et al. [2], which introduces a method that serves to predict alignability based on an analysis of the geometry of point clouds. Risk is defined in this case to quantify the degree to which alignment is constrained, and it is provided on a zero-to-one scale. Both of these methods aim to predict the risk of localization, by relying on different metrics. However, none of these formulations are based on a spatial representation that allows for the construction of a map encoding such risk in different parts of a given environment, which is the focus of this work.

III. ALIGNABILITY MAP

In this section, we provide a brief description of the process that we follow to compute alignability for a given scan, which differs in some aspects from the one in Nobili et al. [2], as explained later on. Then, we show how to use this result to build a complete alignability map. In the scope of this work, each scan obtained from a laser-based sensor will always be a 360-degree three-dimensional point cloud $\mathcal{P}$, although the method would be easy to extend to 2D sensors as well.

The first step of the process consists in the segmentation of the input point cloud into a set of n planar surfaces $\mathbf{P} = \{P_1, P_2, ..., P_n\}$, each one being a subset of points of $\mathcal{P}$. For that, we apply the region growing algorithm described by Rabbani et al. [13], implemented in the PCL library [14]. Each segmented surface will be considered for the process only if its planarity and size are adequate, which we determine by using appropriate thresholds p_{th} and s_{th}, respectively, obtained after different trials. For each $P_i \in \mathbf{P}$, we compute a normalized covariance matrix Σ. Then, we calculate planarity as $p = \lambda_s/\lambda_l$, where λ_s and λ_l are the smallest and largest eigenvalues of Σ, respectively. In the case that $p < p_{th}$, we consider P_i as a planar surface and then compute an oriented bounding box for it, from which we also calculate the area s. Finally, the segmented plane will be accepted if $s > s_{th}$. The values employed for the thresholds are of 0.05 for p_{th} and of $0.01\,m^2$ for s_{th}.

From this process, we get a subset of selected planes $\mathbf{P}_s \subseteq \mathbf{P}$ that will be considered to compute alignability, which is done as follows. First, a normal direction $\mathbf{n}_j = (x_j, y_j, z_j)$ is obtained for each point j of all the planes in $\mathbf{P}_s$, with N the total number of such points. Then, an $N \times 3$ matrix $\mathbf{M}$ in which each row represents a normal $\mathbf{n}_j$ is defined. After that, a principal component analysis (PCA) is performed on matrix $\mathbf{M}$, from which we get three eigenvalues, $\lambda_a \geq \lambda_b \geq \lambda_c \geq 0$. Finally, alignability α can be defined as

$$\alpha = \frac{\lambda_c}{\lambda_a}, \tag{1}$$

where $\alpha \in [0, 1] \subset \mathbb{R}$. In contrast to Nobili et al. [2], we do not consider the overlap between two different point clouds to compute alignability. We can assume that overlap will be high enough as long as a map of the scene is available for localization, which is our use case. Thus, we only compute alignability for a single point cloud instead of doing it for two of them.

With all the above, we can now formally introduce our alignability map, which is based on the metric defined in equation (1). Like in the case of an occupancy grid map, our proposal also relies on a discrete, two-dimensional representation of space. Each cell represents the expected degree of alignability within that region of the map. Thus, an *alignability map* $\mathcal{A}$ is a matrix-based representation of the space in which each cell:

$$\mathcal{A}(i, j) = \text{median}(\mathbf{a}), \tag{2}$$

where $\mathbf{a} = (\alpha_1, \alpha_2, ..., \alpha_n)$ is a vector of n samples of alignability values α_i obtained from point clouds produced by a laser-based sensor placed within the region of the scene corresponding to the considered cell (i, j). To prevent biasing of the alignability score by asymmetric empirical distributions containing outliers, we use robust statistics, i.e., median. Also, for the sake of simplicity, we assume that the sensor has a 360^o field of view, thus, each cell only denotes position. For the case of 3D sensors with a more restricted field of view, the alignability map would have to be defined on different layers, each one representing a different orientation. Furthermore, in the case of 2D sensors, line orientations would be considered instead of plane orientations.

Our alignability map is also tied to the corresponding occupancy grid map of the environment as follows. Let r_{al} and r_{oc} be the resolutions of the alignability and occupancy maps, respectively. Since the value of alignability usually changes only gradually, we allow $r_{\text{al}} \leq r_{\text{oc}}$, with typical numbers being $r_{\text{al}} = 1$ cell/m and $r_{\text{oc}} = 10$ cells/m. Also, the computation in equation (2) is carried out only if occupancy in the corresponding area is low enough. To determine that, we define a maximum level of occupancy $o_{\max}$ beyond which alignability should not be obtained. In the case that $r_{\text{al}} < r_{\text{oc}}$, we calculate the ratio of cells corresponding to the same area in our alignability map that has an occupancy level below $o_{\max}$. This ratio should then not be higher than a certain, appropriate threshold.

IV. VALIDATION

In this section, we demonstrate the utility of our proposal through different experiments. All the tests we describe here have been actually carried out in a virtual environment based on Gazebo and ROS [15], which incorporates a 3D mesh representation of a real environment, a food warehouse in

(a)

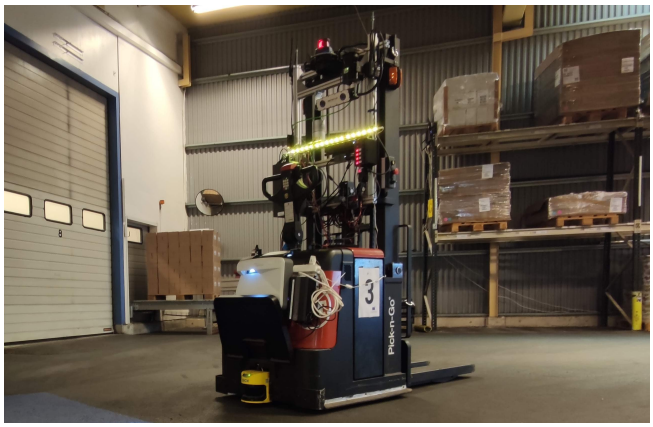

(b)

Fig. 1. Pictures of the real setup used for the experiments. (a) View of the central aisles of the warehouse. (b) View of the robot.

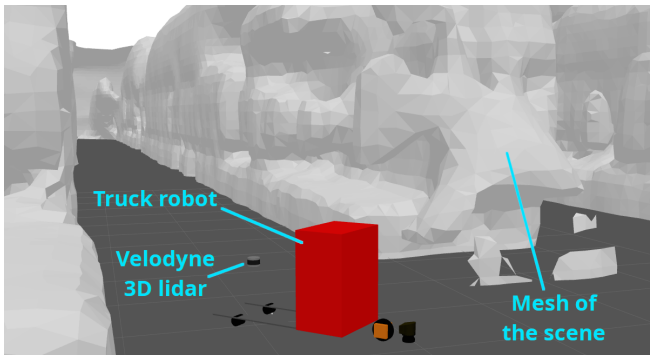

Fig. 2. Three-dimensional view of the virtual environment in Gazebo with the simulated truck robot, pointing towards one of the aisles in figure 1(a), and its 3D lidar sensor.

Sweden (see figure 1(a)). The necessary data for building this mesh has been obtained on-site by using a mobile robot, a Toyota BT SAE200 stacker truck (see figure 1(b)). The truck is endowed with a sensor stack comprising two 2D lidars, one 3D lidar, two RGBD cameras, and an emitrace safety camera[1]. However, only the 3D lidar, a Velodyne HDL-32E has been used in this case. We have also completed our virtual environment with a simulated version of the robot and the 3D lidar sensor (see figure 2).

[1]https://www.retenua.com/en/products/emitrace

In the next subsections, we illustrate the process of creating an alignability map, and we show how alignability can be used as a prediction of the localization error.

A. Building of an alignability map

We have produced an alignability map of the warehouse environment by generating 3D laser scans from several points in the Gazebo model (figure 2), computing their alignability and storing the result in a grid map, following the procedure described in section III. In this case, we aim to illustrate how alignability would be in case of limited sensory capabilities. For that, we have cropped the maximum range of the simulated lidar to only 6.5 meters, which is a much shorter distance than the average length of the aisles in the warehouse (approximately 30 meters). We have used such a limited range to provoke relatively high and noticeable localization errors in some parts of the environment, as we explain in the experiment of section IV-B. The resulting alignability map, with a resolution of 1 meter per cell, is shown in figure 3(a). We have represented alignability values using colors; the redder the lower, and the more blue, the higher (see legend in the figure). It can be noticed from this map that regions with low alignability usually correspond to feature-sparse parts of the scene, like the long corridor B–C, for instance. On the other hand, regions in which there is a higher amount of features (e.g., corners) tend to also have higher alignability, as in the case of corridors A–D or C–D. Thus, we can affirm that the proposed map correctly captures the variety of features in the environment, as expected. However, it can also be observed from figure 3(a) that the highest alignability values in this scene are usually around 0.5. This can be considered good enough to ensure low localization errors, as we show later on. Values close to 1 represent an extreme situation in which a really high amount of different normal directions is observed, which is not necessary for a precise localization, as explained.

B. Alignability as a predictor of localization errors

We have also carried out an experiment in which we aim to analyze the relationship between alignability and localization error. In this experiment, we drive the simulated truck so that it follows a rectangular trajectory, described by waypoints A to D (see figure 3), that is repeated three times. Again, the range of the simulated sensor is limited to 6.5 meters so that the highest localization errors obtained can be noticeable enough, as we show later on. We have estimated the robot position $\mathbf{p}_{est}$ along that path by using NDT-MCL localization [16] and have calculated the error $\mathbf{e}$ with respect to the ground-truth position $\mathbf{p}_{gt}$, provided by Gazebo. We have done this for those cells of the alignability map containing the trajectory followed by the robot. The error for a particular cell (i, j) is calculated as follows:

$$\mathbf{e}(i,j) = \frac{1}{N_s} \sum_{k=1}^{N_s} \|\mathbf{p}_{est}(k) - \mathbf{p}_{gt}(k)\|, \qquad (3)$$

where k denotes a sample of the estimated and ground-truth positions, obtained at the same time, out of a total number

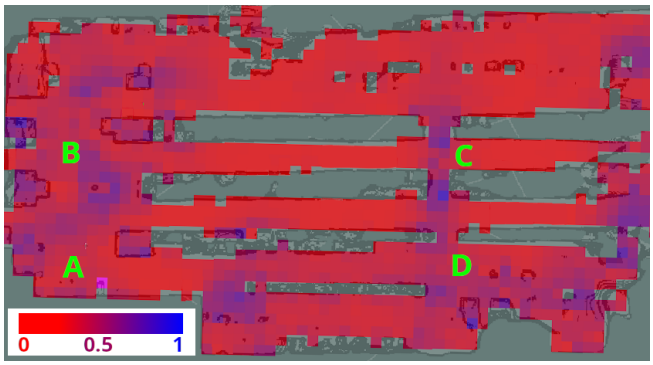

(a)

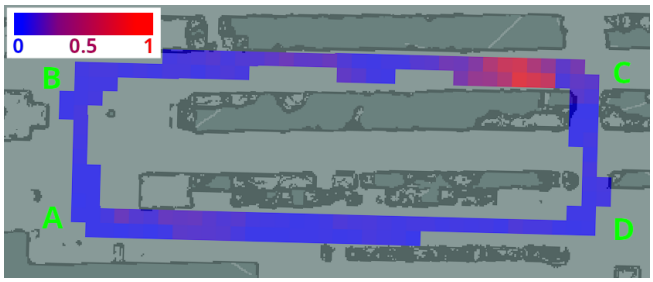

(b)

Fig. 3. (a) Alignability map obtained for the whole food warehouse, with waypoints. Here, colors indicate values of alignability, according to the legend provided (bottom left). (b) Error map obtained during the driving experiment described in the text, with the same waypoints. In this case, colors indicate the ratio of error obtained w.r.t. the maximum one (0.73 meters) on a zero-to-one scale, according to the legend (top left).

of N_s samples in the considered cell. The result is a map of localization errors, which is depicted in figure 3(b). We can observe that the highest errors, around 0.7 meters, are obtained towards the end of corridor B–C, where alignability is also low (see figure 3(a)). As expected, localization error is not very high along the remaining parts of the trajectory (mostly below 0.1 meters) since alignability is good enough. Notice, however, that the error does not immediately increase when entering the low-alignability region of corridor B–C, which is due to the robustness of MCL over time.

The intuition about the influence of alignability on localization error can now be further demonstrated by comparing the predictions from the alignability map (figure 3(a)) to the results shown in the error map (figure 3(b)). For that, we have represented the alignability corresponding to one cell as a function of the error obtained for that cell, which is shown in the scatter plot of figure 4. These results demonstrate that alignability is useful as a predictor of the risk of getting localization errors, as expected. In particular, it can be noticed that alignability is always below 0.1 when the error is high, i.e., when it is greater than 0.3 meters. Also, when alignability is greater than 0.4, localization error is never too high, since it is always less than 0.1 meters.

From the results depicted in figure 4, however, we can further observe that alignability can be low even if errors are also low. The reason behind this is that localization does not immediately deteriorate when suddenly entering a low

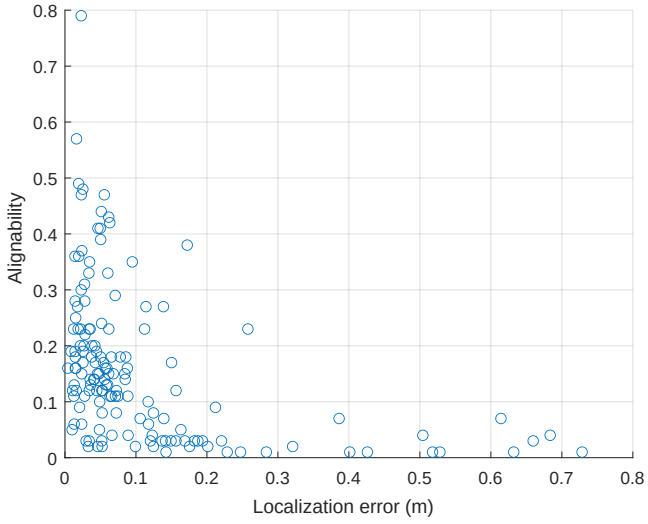

Fig. 4. Scatter plot representing the relationship between alignability and localization error for the driving experiment described in the text. Most of the larger errors are obtained when alignability is below 0.1. In contrast, when it is greater than 0.4, localization errors are always low.

alignability area (e.g., corridor B–C) as explained before. Thus, when alignability is high enough, we can affirm that the risk of localization error is low, and vice versa.

V. CONCLUSIONS AND FUTURE WORK

In this paper we have introduced a grid map that serves to represent the risk of localization error by taking the geometry of the environment into account. The utility of this approach has also been validated across different experiments. We have demonstrated that the proposed map, based on the alignability metric by Nobili et al. [2], correctly captures the amount and variety of features present in the environment, as observed by the robot. Also, we have shown that alignability has a clear influence on localization error and that our map can be used to predict it.

There are also several tasks that we plan to address in future work. One of them is the integration of our alignability map for motion planning, which could serve to generate safe trajectories that minimize the risk of localization error. Also, we plan to extend our approach so that it includes different sources of information for estimating such risk (e.g., information about the dynamics of obstacles in a particular scenario). Finally, we plan to validate our approach for a wider variety of settings, e.g., for outdoor and unstructured environments.

ACKNOWLEDGMENT

This work has received funding from the Swedish Knowledge Foundation (KKS) project ”NiCE” under agreement number 20200247 01 H, and the European Union’s Horizon 2020 research and innovation programme under grant agreement number 101017274.

References

[1] J. Kim, J. Park, and W. Chung. "Self-Diagnosis of Localization Status for Autonomous Mobile Robots". In: *Sensors* 18.9 (Sept. 2018), p. 3168. ISSN: 1424-8220. DOI: 10.3390/s18093168.

[2] S. Nobili, G. Tinchev, and M. Fallon. "Predicting Alignment Risk to Prevent Localization Failure". In: *2018 IEEE International Conference on Robotics and Automation (ICRA)*. 2018, pp. 1003–1010. DOI: 10.1109/ICRA.2018.8462890.

[3] N. Akai, L. Y. Morales, T. Hirayama, and H. Murase. "Misalignment Recognition Using Markov Random Fields With Fully Connected Latent Variables for Detecting Localization Failures". In: *IEEE Robotics and Automation Letters* 4.4 (Oct. 2019), pp. 3955–3962. ISSN: 2377-3766. DOI: 10.1109/LRA.2019.2929999.

[4] C. Cadena, L. Carlone, H. Carrillo, Y. Latif, D. Scaramuzza, J. Neira, I. Reid, and J. J. Leonard. "Past, Present, and Future of Simultaneous Localization and Mapping: Toward the Robust-Perception Age". In: *IEEE Transactions on Robotics* 32.6 (Dec. 2016), pp. 1309–1332. ISSN: 1552-3098. DOI: 10.1109/TRO.2016.2624754.

[5] A. Segal, D. Haehnel, and S. Thrun. "Generalized-ICP". In: *Robotics: Science and Systems V*. Robotics: Science and Systems Foundation, June 2009. ISBN: 9780262514637. DOI: 10.15607/RSS.2009.V.021.

[6] Q. Liao, D. Sun, and H. Andreasson. "Point Set Registration for 3D Range Scans Using Fuzzy Cluster-Based Metric and Efficient Global Optimization". In: *IEEE Transactions on Pattern Analysis and Machine Intelligence* 43.9 (Sept. 2021), pp. 3229–3246. ISSN: 0162-8828. DOI: 10.1109/TPAMI.2020.2978477.

[7] H. Almqvist, M. Magnusson, T. P. Kucner, and A. J. Lilienthal. "Learning to detect misaligned point clouds". In: 35.5 (Aug. 2018), pp. 662–677. DOI: 10.1002/rob.21768.

[8] I. Bogoslavskyi and C. Stachniss. "Analyzing the quality of matched 3D point clouds of objects". In: *2017 IEEE/RSJ International Conference on Intelligent Robots and Systems (IROS)*. IEEE. 2017, pp. 6685–6690.

[9] H. Yin, L. Tang, X. Ding, Y. Wang, and R. Xiong. "A failure detection method for 3D LiDAR based localization". In: *2019 Chinese Automation Congress (CAC)*. IEEE. 2019, pp. 4559–4563.

[10] N. Akai, Y. Akagi, T. Hirayama, T. Morikawa, and H. Murase. "Detection of Localization Failures Using Markov Random Fields With Fully Connected Latent Variables for Safe LiDAR-Based Automated Driving". In: *IEEE Transactions on Intelligent Transportation Systems* (2022), pp. 1–13. DOI: 10.1109/TITS.2022.3164397.

[11] D. Adolfsson, M. Castellano-Quero, M. Magnusson, A. J. Lilienthal, and H. Andreasson. "CorAl: Introspection for robust radar and lidar perception in diverse environments using differential entropy". In: *Robotics and Autonomous Systems* (2022), pp. 104–136. ISSN: 0921-8890. DOI: 10.1016/j.robot.2022.104136.

[12] J. Nubert, E. Walther, S. Khattak, and M. Hutter. *Learning-based Localizability Estimation for Robust LiDAR Localization*. 2022. DOI: 10.48550/ARXIV.2203.05698.

[13] T. Rabbani, F. A. van den Heuvel, and G. Vosselman. "Segmentation of Point Clouds using Smoothness Constraints". In: *International Archives of the Photogrammetry, Remote Sensing and Spatial Information Sciences* 36.5 (2006), pp. 248–253.

[14] R. B. Rusu and S. Cousins. "3D is here: Point Cloud Library (PCL)". In: *2011 IEEE International Conference on Robotics and Automation*. IEEE, May 2011, pp. 1–4. ISBN: 978-1-61284-386-5. DOI: 10.1109/ICRA.2011.5980567.

[15] M. Quigley, K. Conley, B. Gerkey, J. Faust, T. Foote, J. Leibs, R. Wheeler, and A. Y. Ng. "ROS: an open-source Robot Operating System". In: *ICRA workshop on open source software*. 2009.

[16] J. Saarinen, H. Andreasson, T. Stoyanov, and A. Lilienthal. "Normal Distribution Transform Monte-Carlo Localization (NDT-MCL)". In: *Proc. IEEE/RSJ Int. Conf. on Intell. Robots and Syst.* 2013, pp. 382–389.